

A Nonlocal Homogenization Model for Wave Dispersion in Dissipative Composite Materials

Tong Hui and Caglar Oskay*

Department of Civil and Environmental Engineering
Vanderbilt University
Nashville, TN 37235

Abstract

This manuscript presents a nonlocal homogenization model for the analysis of wave dispersion and energy dissipation in bimaterial viscoelastic composites subjected to dynamic loading conditions. The proposed model is derived based on the asymptotic homogenization method with multiple spatial scales applied in the Laplace domain. Asymptotic expansions of the associated response fields up to fourth order are employed to account for wave dispersions induced by the microscopic heterogeneities. The solution of the nonlocal homogenization approach is obtained in semi-analytical form in the Laplace domain and discrete inverse Laplace transform method is employed to approximate the response fields in the time domain. Numerical examinations are carried out to verify the proposed model and assess its capabilities compared to the standard (i.e., local) homogenization and the analytical solutions of composite beams subjected to dynamic loading conditions. Investigations reveal that the nonlocal model accurately accounts for wave dispersions and heterogeneity induced attenuation. A parametric analysis is conducted to identify the relationship between microstructure and heterogeneity induced attenuation under high-frequency loading.

Keywords: Multiscale modeling; Computational homogenization; Composites; Wave dispersion; Energy dissipation.

*Corresponding author address: VU Station B#351831, 2301 Vanderbilt Place, Nashville, TN 37235. Email: caglar.oskay@vanderbilt.edu

1 Introduction

Composites and other heterogeneous materials exhibit complex response patterns when subjected to dynamic loading conditions due to the intrinsic wave interactions at the interfaces between material constituents. The complexity of the dynamic response in heterogeneous materials also provides tremendous opportunities for devising tailored microstructures with optimal functional characteristics such as cloaking, impact and blast resistance, health monitoring and others. The development of such tailored microstructures for optimal performance requires a deeper understanding of the pertinent microstructure - property relationships. This research is aimed at understanding the relationship between the material microstructure and energy dissipation characteristics of viscoelastic bimaterial composites for impact and blast response applications. We particularly focus on modeling energy dissipation and wave dispersion phenomena in dynamic response of heterogeneous viscoelastic materials.

It is well known that heterogeneous materials exhibit wave dispersion when the characteristic length of the traveling waves approach the size of the material microstructure (Porubov et al., 2009; Rubin et al., 1995), altering the shape and velocity of propagating waves. The realization of this phenomena dates back to the classical works of Cosserat and Cosserat (Cosserat and Cosserat, 1909), Mindlin (Mindlin, 1964), and Eringen (Eringen and Suhubi, 1964). The effects of micro-inertia and dispersion have been recently modeled using a number of approaches such as gradient enhancement (Bennett et al., 2007), time-harmonic Bloch expansions (Santosa and Symes, 1991), scale bridging through Hamilton's principle (Wang and Sun, 2002), and models based on Mindlin's theory (Engelbrecht et al., 2005; Gonella et al., 2011). These approaches typically involve incorporation of high order strain and inertia gradient terms to the macroscopic equations of motion, which has been demonstrated to be effective in the context of stiff composites undergoing small deformations.

Mathematical homogenization provides an alternative approach for modeling wave dispersion in heterogeneous materials. Rooted in the works of Sánchez-Palencia (1980); Bensoussan et al. (1978); Bakhvalov and Panasenko (1989) and others, mathematical homogenization has been used to evaluate the mechanical response of heterogeneous materials under static and

quasi-static loading, as well as dynamic problems involving long wavelengths compared to the characteristic size of the heterogeneity (e.g., (Guedes and Kikuchi, 1990; Terada and Kikuchi, 1995; Crouch and Oskay, 2010)). The theory of mathematical homogenization with multiple spatial and temporal scales has also been employed to devise dispersion models for dynamic response of linear elastic heterogeneous materials in the context of one-dimensional and multi-dimensional problems (Chen and Fish, 2001; Fish et al., 2002a; Bakhvalov and Eglit, 2005; Andrianov et al., 2008). In principle, wave dispersion effects are introduced by considering high order terms in the asymptotic expansion of the response fields. The models derived based on the mathematical homogenization theory were shown to accurately account for wave dispersions.

In contrast to the elastic dispersion models, the literature on modeling the dynamic behavior of dispersive viscoelastic composites is relatively scarce. Chin-Teh (1971) investigated the propagation of transient cylindrical shear waves in functionally graded viscoelastic bodies, in which the creep function varies along the radial direction. Wave propagation was modeled using the theory of propagating surfaces of discontinuities. Nayfeh (1974) used a discrete lattice model to simulate transient response of periodic, semi-infinite, elasto-viscoelastic composites. The dispersive solution was obtained by resolving the characteristic equations for the lattice model in the Laplace domain and subsequently transforming the solution to the time domain. Ting (1980) carried out an investigation of a semi-infinite periodic layered composite where two viscoelastic materials are alternately positioned. The Laplace transform and asymptotic expansion of the relaxation modulus are used to achieve the dispersive solution. Mukherjee and Lee (1975) conducted an analysis of the dispersion and mode shapes for free vibrations in infinite laminated media. The complex modulus formulation was employed to linearize the governing differential equations. A finite difference discretization and quasi periodic boundary conditions were used to solve the complex eigenvalue problem. More recently, plane harmonic waves in unbounded periodic viscoelastic composite materials were investigated by Naciri et al. (1994). The complex modulus function based governing equations were solved using the finite element method to investigate the relationship between damping and dispersion. Abu-Alshaikh et al. (2001) considered two dimensional transient waves propagat-

ing in an N -layer viscoelastic medium idealized by a two-term Prony series. The governing hyperbolic equations in the Fourier domain were transformed to canonical equations by the method of characteristics and the solutions were obtained using step-by-step integration. Tsai and Prakash (2005) investigated the decay in the elastic precursor and late time dispersion of weak shock waves in layered composites based on the Laplace transform associated with Floquet’s theorem. Jiangong (2011) idealized the response of shear waves with the Kelvin-Voigt model in functionally graded viscoelastic plates. The dispersive solution was obtained by approximating the response fields using a Legendre orthogonal polynomial series.

Despite the seminal contributions on modeling and characterization of the dynamic response of viscoelastic heterogeneous materials, modeling the effect of microstructure induced dispersion on the dissipative characteristics of viscous composites, a key fundamental knowledge for devising tailored microstructures for impact and blast mitigation, remains to be identified. In this manuscript, we propose a one-dimensional nonlocal homogenization model for the relationship between microstructure and energy dissipation characteristics of a bimaterial composite. The present work applies the mathematical homogenization theory with multiple scales in the Laplace domain to formulate the nonlocal model. To the best of the authors’ knowledge, previous dispersion models based on mathematical homogenization theory have been only applied to problems defined in the time domain and for elastic material response. Fourth order asymptotic expansions are used to account for the microscopic dynamics causing dispersion, and the microscopic spatial coordinate is eliminated in the governing equations avoiding the expensive computation at multiple spatio-temporal scales. Fourth is the lowest order in the asymptotic series (hence the simplest and most efficient model within the model hierarchy) with which, the wave dispersion and the dispersion induced wave attenuation can be modeled. It is possible to construct higher order homogenization models through the inclusion of additional terms in the asymptotic expansions. For instance, Fish and Chen (2001) investigated fourth and sixth order homogenization models in the context of elastic composites. While the higher (i.e., sixth) order terms increase accuracy in capturing the dispersion effects, the fourth order model was shown to be accurate in the range of applicability of the homogenization approach, which is controlled by the impedance mismatch, ratio between the

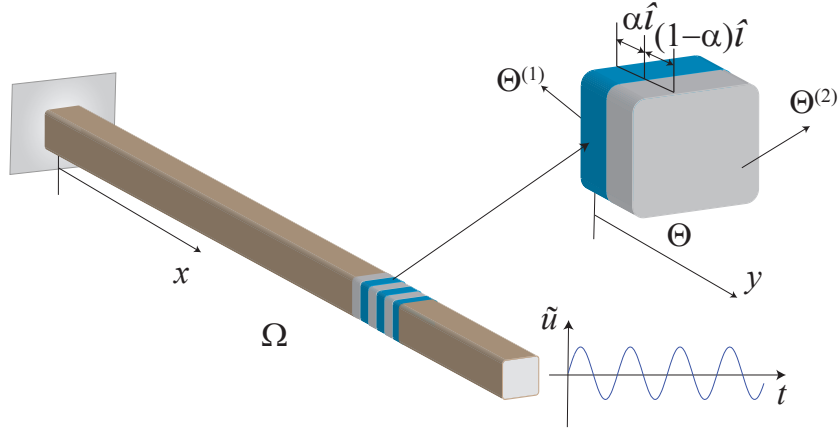


Figure 1: Problems at macroscale and microscale.

micro- and macrostructure size, as well as impulse characteristics. The solution of the nonlocal homogenization approach is obtained in the semi-analytical form in the Laplace domain and discrete inverse Laplace transform method is employed to approximate the response fields in the time domain. The capabilities of the proposed model are verified against the analytical solution and the classical (local) homogenization model for accuracy and computational cost. A parametric analysis is conducted to identify the relationship between microstructure and heterogeneity induced attenuation under high frequency loading.

The remainder of this manuscript is organized as follows: Section 2 presents the description of the multiscale problem in the time and Laplace domains. Section 3 derives the governing equations for the nonlocal homogenization model based on the high-order asymptotic expansion method in the Laplace domain. Section 4 presents the solution methodologies employed to evaluate the nonlocal and local homogenization models as well as direct analytical evaluation of the governing equations of motion. This section also provides the implementation of dissipated energy computation and the discrete inverse Laplace transform method. Section 5 includes numerical results for heterogeneous beam structures subjected to step and sinusoidal boundary conditions, and concluding remarks are presented in Section 6.

2 Problem Setting

Consider a one-dimensional bimaterial heterogeneous body as illustrated in Fig. 1. The domain of the body, $\Omega = [0, L]$ is formed by the repetition of a locally periodic microstructure, Θ . The size of the material microstructure is taken to be small compared to the overall size of the macroscopic domain. Denoting x and y as the position coordinates at the scales of the macro- and microstructures, respectively, the two scales are related by a small scaling parameter: $y = x/\zeta$; where, $0 < \zeta \ll 1$ is the ratio between the characteristic size of the microstructure and the length of the traveling waves along the heterogeneous body.

Let $f^\zeta(x, t)$ be an arbitrary response field, which oscillates in space due to fluctuations induced by the material heterogeneity. We consider the following two scale decomposition of the original single position coordinate:

$$f^\zeta(x, t) = f(x, y(x), t) \quad (1)$$

where, superscript ζ indicates the dependence of the response field on the microstructural heterogeneity; and, t denotes time. The spatial derivative of f^ζ is computed by the chain rule as:

$$f^\zeta_{,x}(x, t) = f_{,x}(x, y, t) + \frac{1}{\zeta} f_{,y}(x, y, t) \quad (2)$$

where, a subscript followed by a comma denotes differentiation, repeated subscripts denotes higher order differentiation. The response fields are taken to be spatially periodic throughout the deformation process:

$$f(x, y, t) = f(x, y + \hat{l}, t); \quad \forall x \in \Omega \quad (3)$$

in which, \hat{l} denotes the period of the microstructure in the stretched coordinate system, y (Fig. 1).

2.1 Governing equations in the time domain

In the time domain, the deformation response of the heterogeneous body subjected to dynamic loading conditions is governed by the momentum balance equation in the form:

$$\sigma_{,x}^{\zeta}(x, t) = \rho^{\zeta}(x)u_{,tt}^{\zeta}(x, t) \quad (4)$$

in which, σ^{ζ} and u^{ζ} are the stress and displacement fields, respectively; and, ρ^{ζ} denotes density. A generalized viscoelastic model described by the Duhamel's integral is employed to provide the constitutive response of the material constituents:

$$\sigma^{\zeta}(x, t) = \int_0^t g^{\zeta}(x, t - \tau)\epsilon_{,\tau}^{\zeta}(x, \tau)d\tau \quad (5)$$

where, g^{ζ} is the modulus function; and, ϵ^{ζ} denotes the strain field, assuming small strain kinematics:

$$\epsilon^{\zeta}(x, t) = u_{,x}^{\zeta}(x, t) \quad (6)$$

The dynamic loads are imparted on the heterogeneous body based on prescribed displacements along the boundaries of the domain. We consider the following initial and boundary conditions:

$$u^{\zeta}(x, 0) = u^0(x); \quad v^{\zeta}(x, 0) = v^0(x) \quad (7)$$

$$u^{\zeta}(0, t) = 0; \quad u^{\zeta}(L, t) = \tilde{u}(t) \quad (8)$$

in which, L is the length of the heterogeneous body; $v^{\zeta} = u_{,t}^{\zeta}$ the velocity field; and, u^0 , v^0 and \tilde{u} are prescribed initial and boundary data.

2.2 Governing equations in the Laplace domain

The particular forms of the generalized viscoelastic constitutive model and the momentum balance equation permit a simpler description of the governing boundary value problem in the Laplace domain. In this section, we introduce the key characteristics of the Laplace transform

employed in the formulation and recast the governing system of equations in the Laplace domain.

The Laplace transform of an arbitrary, real valued, time varying function, $f \in \mathbb{R}$, is defined as:

$$\bar{f}(s) \equiv \mathcal{L}(f(t)) = \int_0^{\infty} e^{-st} f(t) dt \quad (9)$$

where, the Laplace argument, s and the Laplace transform, \bar{f} , are complex valued (i.e., $s \in \mathbb{C}$ and $\bar{f} := \mathbb{C} \rightarrow \mathbb{C}$). Overbar on a response function indicates the Laplace transform, and the representation of a function or an equation in the Laplace domain is referred to as *associated* function or equation throughout the remainder of this manuscript. The derivative rule for the Laplace transform is given as:

$$\mathcal{L}(\underbrace{f, tt \dots t}_{n \text{ times}}(t)) = s^n \bar{f}(s) - s^{n-1} f(0) - \dots - \underbrace{f, tt \dots t}_{n-1 \text{ times}}(0) \quad (10)$$

and the convolution integral rule is given as:

$$\mathcal{L}\left(\int_0^t f_1(t-\xi) f_2(\xi) d\xi\right) = \mathcal{L}\left(\int_0^t f_1(\xi) f_2(t-\xi) d\xi\right) = \mathcal{L}(f_1) \mathcal{L}(f_2) \quad (11)$$

Considering a statically undeformed initial condition (i.e., $u^0(x) = v^0(x) = 0$), taking the Laplace transform of the momentum balance equation (Eq. 4) and employing the derivative rule for the Laplace transform (Eq. 10) yield the associated momentum balance equation:

$$\bar{\sigma}_{,x}^{\zeta}(x, s) = \rho^{\zeta}(x) s^2 \bar{u}^{\zeta}(x, s) \quad (12)$$

Applying the convolution integral rule (Eq. 11) to the constitutive equation of the viscoelastic constituents (Eq. 5) and using Eq. 10 yield the associated constitutive law:

$$\bar{\sigma}^{\zeta}(x, s) = E^{\zeta}(x, s) \bar{\epsilon}^{\zeta}(x, s) \quad (13)$$

in which, the associated modulus function in the Laplace domain, E^{ζ} , is related to the modulus

function, g^ζ as:

$$E^\zeta(x, s) = s\mathcal{L}\left(g^\zeta(x, t)\right) \quad (14)$$

Taking the Laplace transform of the boundary conditions yields the associated boundary conditions:

$$\bar{u}^\zeta(0, s) = 0; \quad \bar{u}^\zeta(L, s) = \hat{u}(s) \quad (15)$$

in which, \hat{u} is the Laplace transform of the known boundary data, \tilde{u} . The governing equations of the dynamic response of the heterogeneous body defined in the Laplace domain is summarized in Box 1.

Given ρ^ζ , E^ζ , and \hat{u} ; find $\bar{u}^\zeta \in \mathbb{C}$ such that in $x \in \Omega$ and $s \in \mathbb{C}$

Momentum balance: $\bar{\sigma}_{,x}^\zeta(x, s) = \rho^\zeta(x)s^2\bar{u}^\zeta(x, s)$

Kinematics equation: $\bar{\epsilon}^\zeta(x, s) = \bar{u}_{,x}^\zeta(x, s)$

Constitutive equation: $\bar{\sigma}^\zeta(x, s) = E^\zeta(x, s)\bar{u}_{,x}^\zeta(x, s); \quad E^\zeta(x, s) = s\mathcal{L}\left(g^\zeta(x, t)\right)$

Boundary conditions $\bar{u}^\zeta(0, s) = 0; \quad \bar{u}^\zeta(L, s) = \hat{u}(s)$

Box 1: Governing boundary value problem in the Laplace domain.

The density and modulus are taken to vary as a function of the microscale coordinates only. For a bimaterial microstructure:

$$E^\zeta = E(y, s) = \begin{cases} E_1(s) & \text{if } y \in \Theta^{(1)} \\ E_2(s) & \text{if } y \in \Theta^{(2)} \end{cases} \quad (16)$$

$$\rho^\zeta = \rho(y) = \begin{cases} \rho_1 & \text{if } y \in \Theta^{(1)} \\ \rho_2 & \text{if } y \in \Theta^{(2)} \end{cases} \quad (17)$$

where, $\Theta^{(1)}$ and $\Theta^{(2)}$ are the domains of phases 1 and 2, respectively, such that $\Theta = \Theta^{(1)} \cup \Theta^{(2)}$; and, $\{E_1, \rho_1\}$ and $\{E_2, \rho_2\}$ are the material parameters defining the corresponding phases.

3 Nonlocal Homogenization

In this section, a nonlocal homogenization model is devised for the dynamic response of viscoelastic bimaterial composites by applying the mathematical homogenization theory with multiple spatial scales on the governing equations defined in the Laplace domain. The derivation follows the procedure originally proposed by Fish et al. (2002b), who devised a nonlocal homogenization model for linear elastic bimaterial composites by employing the mathematical homogenization theory in the time domain.

We start by approximating displacement based on the asymptotic expansion of the form:

$$u^\zeta(x, t) \equiv u(x, y, t) = u_0(x, t) + \zeta u_1(x, y, t) + \zeta^2 u_2(x, y, t) + \zeta^3 u_3(x, y, t) + O(\zeta^4) \quad (18)$$

where, u_0 denotes the macroscopic displacement field and is independent of the microstructure; and, u_i are spatially oscillatory high-order displacement fields. By linearity of the Laplace transform, the associated displacement field is also expressed in terms of the asymptotic series:

$$\bar{u}(x, y, s) = \bar{u}_0(x, s) + \zeta \bar{u}_1(x, y, s) + \zeta^2 \bar{u}_2(x, y, s) + \zeta^3 \bar{u}_3(x, y, s) + O(\zeta^4) \quad (19)$$

Substituting Eq. 19 into the associated constitutive law (Eq. 13), the stress-strain relationships at any order are obtained as:

$$O(\zeta^i) : \quad \bar{\sigma}_i(x, y, s) = E(y, s)(\bar{u}_{i,x} + \bar{u}_{i+1,y}); \quad i = 0, 1, \dots \quad (20)$$

Substituting Eq. (19) and the constitutive equations at various orders (Eq. 20) into the associated momentum balance equation (Eq. 12), the momentum balance equations of orders

$O(\zeta^{-1})$ to $O(\zeta^2)$ are expressed as:

$$O(\zeta^{-1}) : \quad [E(y, s)(\bar{u}_{0,x} + \bar{u}_{1,y})]_{,y} = 0 \quad (21)$$

$$O(1) : \quad \rho(y)\bar{u}_0 s^2 - [E(y, s)(\bar{u}_{0,x} + \bar{u}_{1,y})]_{,x} - [E(y, s)(\bar{u}_{1,x} + \bar{u}_{2,y})]_{,y} = 0 \quad (22)$$

$$O(\zeta) : \quad \rho(y)\bar{u}_1 s^2 - [E(y, s)(\bar{u}_{1,x} + \bar{u}_{2,y})]_{,x} - [E(y, s)(\bar{u}_{2,x} + \bar{u}_{3,y})]_{,y} = 0 \quad (23)$$

$$O(\zeta^2) : \quad \rho(y)\bar{u}_2 s^2 - [E(y, s)(\bar{u}_{2,x} + \bar{u}_{3,y})]_{,x} - [E(y, s)(\bar{u}_{3,x} + \bar{u}_{4,y})]_{,y} = 0 \quad (24)$$

Considering the balance equations at the lower two orders (Eqs. 21 and 22) leads to the classical homogenization model (e.g. Oskay and Fish, 2007). The classical homogenization model is local in character and valid only when displacement wavelengths are large enough that the wave reflections along the bimaterial interfaces are negligible. The $O(\zeta)$ and $O(\zeta^2)$ balance equations introduce high order terms in the resulting homogenized equations, leading to a nonlocal homogenization model that can account for the dispersion induced by wave reflections at material microstructure boundaries.

Consider the $O(\zeta^{-1})$ associated boundary value problem (Eq. 21). By linearity, the first order microscale associated displacement field, \bar{u}_1 , is expressed using the following decomposition:

$$\bar{u}_1(x, y, s) = \bar{U}_1(x, s) + H(y, s)\bar{u}_{0,x}(x, s) \quad (25)$$

where, H denotes the first order microscopic influence function providing the oscillatory component of \bar{u}_1 , whereas \bar{U}_1 denotes the macroscopic contribution of \bar{u}_1 . Applying Eq. 25 to Eq. 21, a linear equilibrium equation for the first order microscopic influence function is obtained:

$$\{E(y, s)(1 + H_{,y})\}_{,y} = 0 \quad (26)$$

Equation 26 is evaluated by imposing the periodicity, continuity and normality conditions. The periodicity of the influence function follows from the periodicity of the displacement field:

$$H(y = 0, s) = H(y = \hat{l}, s); \quad \bar{\sigma}_0(x, y = 0, s) = \bar{\sigma}_0(x, y = \hat{l}, s) \quad (27)$$

in which, $\hat{l} = l/\zeta$; and, l is the physical length of the microstructure. The continuity of the microscale response fields across the bimaterial interfaces are ensured by imposing the following constraints:

$$\lim_{\nu \rightarrow 0} H(y = \alpha\hat{l} + \nu^+, s) - H(y = \alpha\hat{l} - \nu^-, s) = 0 \quad (28)$$

$$\lim_{\nu \rightarrow 0} \bar{\sigma}_0(x, y = \alpha\hat{l} + \nu^+, s) - \bar{\sigma}_0(x, y = \alpha\hat{l} - \nu^-, s) = 0 \quad (29)$$

where, $0 \leq \alpha \leq 1$ is the volume fraction of phase 1 in the bimaterial microstructure as shown in Fig. 1. The uniqueness of the influence function is ensured by imposing the normality condition on the microscale associated displacement field, \bar{u}_1 :

$$\langle \bar{u}_1(x, y, s) \rangle = \bar{U}_1(x, s) \rightarrow \langle H(y, s) \rangle = 0 \quad (30)$$

where, MacCauley brackets, $\langle \cdot \rangle$, denote the spatial averaging over the microstructure:

$$\langle f \rangle = \frac{1}{|\Theta|} \int_{\Theta} f(x, y, s) dy \quad (31)$$

where, $|\cdot|$ is the size of the microstructural domain (i.e., $|\Theta| = \hat{l}$). Considering the constraints in Eqs. 27-30, the influence function is evaluated in a closed form as follows,

$$H(y, s) = \begin{cases} \frac{(1-\alpha)(E_2(s) - E_1(s))}{(1-\alpha)E_1(s) + \alpha E_2(s)} \left(y - \frac{\alpha\hat{l}}{2} \right); & y \in \Theta^{(1)} \\ \frac{\alpha(E_1(s) - E_2(s))}{(1-\alpha)E_1(s) + \alpha E_2(s)} \left(y - \frac{(1+\alpha)\hat{l}}{2} \right); & y \in \Theta^{(2)} \end{cases} \quad (32)$$

The $O(1)$ homogenized equilibrium equation is obtained by applying the averaging operator (Eq. 31) to the associated balance equation (Eq. 22). Considering the periodicity of the first order associated microscopic stress, $\bar{\sigma}_1$ yields:

$$\rho_0 \bar{u}_0 s^2 - E_0(s) \bar{u}_{0,xx} = 0 \quad (33)$$

where, ρ_0 and $E_0(s)$ denote the homogenized density and homogenized associated modulus

function, respectively:

$$\rho_0 \equiv \langle \rho \rangle = \alpha \rho_1 + (1 - \alpha) \rho_2 \quad (34)$$

$$E_0(s) = \langle E(y, s)(1 + H_{,y}) \rangle = \frac{E_1(s)E_2(s)}{(1 - \alpha)E_1(s) + \alpha E_2(s)} \quad (35)$$

Next, we consider the $O(1)$ associated momentum balance equation (Eq. 22). Substituting Eqs. 25 and 33 into Eq. 22 yields:

$$\{E(y, s)(\bar{u}_{2,y} + \bar{U}_{1,x} + H\bar{u}_{0,xx})\}_{,y} = \{(\theta(y) - 1)E_0\} \bar{u}_{0,xx} \quad (36)$$

where, $\theta(y) = \rho(y)/\rho_0$. By linearity, the second order microscale associated displacement field, \bar{u}_2 is expressed as:

$$\bar{u}_2(x, y, s) = \bar{U}_2(x, s) + H(y, s)\bar{U}_{1,x}(x, s) + P(y, s)\bar{u}_{0,xx}(x, s) \quad (37)$$

in which, $P(y, s)$ is the second order microscale influence function. Considering the periodicity, continuity and normality constraints, P is uniquely evaluated by Eq. 36 in closed form. Employing the closed form expression for the second order microscale influence function and considering the periodicity of the second order stress field, $\bar{\sigma}_2$, the $O(\zeta)$ homogenized momentum balance equation is obtained by applying the averaging operator to Eq. 23:

$$\rho_0 \bar{U}_1 s^2 - E_0 \bar{U}_{1,xx} = 0 \quad (38)$$

The third order associated microscale displacement field, \bar{u}_3 is determined using the $O(\zeta)$ momentum balance equation (Eq. 23). Decompositions of the lower order microscale displacement fields (Eqs. 25 and 37) and the homogenized balance equations (Eqs. 33 and 38) at $O(1)$ and $O(\zeta)$ are substituted into Eq. 23 to yield:

$$\begin{aligned} & \{E(y, s)(\bar{u}_{3,y} + \bar{U}_{2,x} + H(y, s)\bar{U}_{1,xx} + P(y, s)\bar{u}_{0,xxx})\}_{,y} \\ & = \{\theta(y)E_0(s)H(y, s) - E(y, s)(H + P_{,y})\} \bar{u}_{0,xxx} + \{(\theta(y) - 1)E_0(s)\} \bar{U}_{1,xx} \quad (39) \end{aligned}$$

We consider the following form for the third order associated microscale displacement field:

$$\bar{u}_3(x, y, s) = \bar{U}_3(x, s) + H(y, s)\bar{U}_{2,xx} + P(y, s)\bar{U}_{1,xxx} + Q(y, s)\bar{u}_{0,xxx} \quad (40)$$

where, $Q(y, s)$ is the third order microscale influence function. Analogous to the evaluation of the lower order influence functions, Q is uniquely determined from the $O(\zeta)$ momentum balance equation provided that the periodicity, continuity and normality conditions are imposed.

The $O(\zeta^2)$ homogenized momentum balance equation is obtained by applying the averaging operator to Eq. 24 and utilizing the expressions of $P(y, s)$ and $Q(y, s)$:

$$\rho_0\bar{U}_2s^2 - E_0\bar{U}_{2,xx} = \frac{1}{\zeta^2}E_d\bar{u}_{0,xxxx} \quad (41)$$

where,

$$E_d(s) = \frac{[\alpha(1-\alpha)]^2(E_1\rho_1 - E_2\rho_2)^2E_0l^2}{12\rho_0^2[(1-\alpha)E_1 + \alpha E_2]^2} \quad (42)$$

Consider the average associated displacement field up to $O(\zeta^3)$:

$$\bar{U}(x, s) = \langle \bar{u}(x, y, s) \rangle = \bar{u}_0(x, s) + \zeta\bar{U}_1(x, s) + \zeta^2\bar{U}_2(x, s) + O(\zeta^3) \quad (43)$$

Summing the homogenized momentum balance equations at orders $O(1)$, $O(\zeta)$, and $O(\zeta^2)$ (Eqs. 33, 38 and 41), a governing homogenized balance equation for \bar{U} is obtained in the following form:

$$\rho_0s^2\bar{U} - E_0\bar{U}_{,xx} - E_d\bar{U}_{,xxxx} = 0 \quad (44)$$

It is important to note that the dispersive behavior is captured due to the presence of the last term in Eq. 44. The coefficient E_d introduces a characteristic length term (proportional to l^2). Introducing the dispersive term in the governing equation leads to a fourth order ordinary differential equation for the evaluation of associated homogenized displacement field, $\bar{U}(x, s)$ in the Laplace domain. This is in contrast to the time domain analysis by Fish et al. (2002b), which leads to a partial differential equation for the evaluation of the homogenized displacement field in the time domain. Since the governing equation is of the fourth order, the

boundary conditions of the original initial boundary value problem provided in Eq. 15 is not sufficient to uniquely determine \bar{U} . We therefore consider two additional artificial boundary conditions:

$$\bar{U}_{,xx}(0, s) = 0, \quad \bar{U}_{,xxx}(L, s) = 0 \quad (45)$$

The resulting boundary value problem for the homogenized nonlocal response of the heterogeneous body subjected to the dynamic loads is summarized in Box 2.

Given ρ^ζ , E^ζ , and \hat{u} ; find $\bar{U} \in \mathbb{C}$ such that in $x \in \Omega$ and $s \in \mathbb{C}$

Macro-homogenized equilibrium equation: $\rho_0 s^2 \bar{U} - E_0 \bar{U}_{,xx} - E_d \bar{U}_{,xxxx} = 0$

Essential boundary conditions: $\bar{U}(0, s) = 0 \quad \bar{U}(L, s) = \hat{u}(s)$

Additional boundary conditions: $\bar{U}_{,xx}(0, s) = 0 \quad \bar{U}_{,xxx}(L, s) = 0$

Box 2: Governing boundary value problem for the nonlocal homogenization model.

4 Solution Procedures

This section provides the analytical solutions of the nonlocal homogenization model, the classical homogenization model and the direct single scale boundary value problem. The computation of the dissipated energy density at a material point in the Laplace domain and the discrete Laplace transform method employed to describe the computed response fields in the time domain are presented.

4.1 Homogenization models

The fourth order ordinary differential equation for the nonlocal homogenization model provided in Box 2 is analytically evaluated by considering the following form for the homogenized displacement field:

$$\bar{U}(x, s) = A(s) \sinh(\xi x) + B(s) \sinh(\eta x) \quad (46)$$

in which, the coefficients, A , B , ξ and η are obtained using the boundary conditions as:

$$A(s) = \frac{\hat{u}(s) \eta^3}{(\eta^3 - \xi^3) \sinh(\xi L)}; \quad B(s) = \frac{\hat{u}(s) \xi^3}{(\xi^3 - \eta^3) \sinh(\eta L)} \quad (47a)$$

$$\xi = \sqrt{\frac{-E_0 + \sqrt{E_0^2 + 4\rho_0 E_d s^2}}{2E_d}}; \quad \eta = \sqrt{\frac{-E_0 - \sqrt{E_0^2 + 4\rho_0 E_d s^2}}{2E_d}} \quad (47b)$$

When homogenization is conducted up to order $O(\zeta)$, the formulation described in Section 3 leads to the classical homogenization model governed by the following second order ordinary differential equation:

$$\rho_0 s^2 \bar{u}_0 - E_0 \bar{u}_{0,xx} = 0 \quad (48)$$

Equation 48 is evaluated analytically using the following form:

$$\bar{u}_0(x, s) = C(s) \sinh(\varphi x) \quad (49)$$

The coefficients C and φ are obtained using the boundary conditions as follows:

$$C(s) = \frac{\hat{u}(s)}{\sinh(\varphi L)}; \quad \varphi = \frac{\text{sign}(\text{Re}(s))}{V_0} s; \quad V_0 = \sqrt{\frac{E_0}{\rho_0}} \quad (50)$$

where, V_0 is the frequency dependent homogenized velocity.

4.2 Original governing equations

Given ρ_i , E_i and \hat{u} ; find $\bar{u}_i^n \in \mathbb{C}$ such that in $x \in \Omega$ and $s \in \mathbb{C}$	
Equilibrium equation:	$E_i \bar{u}_{i,x_i x_i}^n(x_i, s) = \rho_i s^2 \bar{u}_i^n(x_i, s)$
Constitutive equation:	$\bar{\sigma}_i^n(x_i, s) = E_i \bar{u}_{i,x_i}^n(x_i, s)$
Continuous conditions at interfaces:	$\bar{u}_1^n(\alpha l, s) = \bar{u}_2^n(0, s) \quad \bar{u}_2^n((1 - \alpha)l, s) = \bar{u}_1^{n+1}(0, s)$
	$\bar{\sigma}_1^n(\alpha l, s) = \bar{\sigma}_2^n(0, s) \quad \bar{\sigma}_2^n((1 - \alpha)l, s) = \bar{\sigma}_1^{n+1}(0, s)$
Boundary conditions:	$\bar{u}_1^1(0, s) = 0 \quad \bar{u}_2^N((1 - \alpha)l, s) = \hat{u}(s)$

Box 3: Summary of the boundary value problem for the n^{th} microstructure

In this section, we derive the analytical solution of the original governing boundary value problem summarized in Box 3. The analytical solution derived in this section is employed as the reference solution in the numerical simulations that are discussed in the subsequent sections. The analytical solution is obtained by exploiting the governing equation on each phase of each microstructure along the heterogeneous body and enforcing continuity across each bimaterial interface.

We start by numbering microstructures along the beam. At the n^{th} microstructure ($n = 1, \dots, N$, where N denotes total number of microstructures). We define two position coordinates x_1 and x_2 to parameterize the phase domains $\Omega_1^n = [0, \alpha l]$ and $\Omega_2^n = [0, (1 - \alpha)l]$, respectively. The boundary value problem for each phase of the n^{th} microstructure including the continuity conditions for the displacements, \bar{u}_i^n and stresses, $\bar{\sigma}_i^n$ at the interfaces are summarized in Box 3.

The general solution for the equilibrium equation in the boundary value problem is:

$$\bar{u}_i^n(x, s) = A_i^n \exp(\gamma_i x) + B_i^n \exp(-\gamma_i x) \quad (51)$$

with,

$$\gamma_i = \frac{\text{sign}(\text{Re}(s))}{V_i}; \quad V_i = \sqrt{\frac{E_i}{\rho_i}} \quad (52)$$

where, V_i is the complex wave velocity of phase i . The displacement and stress fields at the boundaries of each phase of the n^{th} microstructure read,

$$\bar{u}_1^n(0, s) = A_1^n + B_1^n, \quad \bar{\sigma}_1^n(0, s) = A_1^n \eta_1 - B_1^n \eta_1 \quad (53)$$

$$\bar{u}_1^n(\alpha l, s) = A_1^n \xi_1 + B_1^n / \xi_1, \quad \bar{\sigma}_1^n(\alpha l, s) = A_1^n \eta_1 \xi_1 - B_1^n \eta_1 / \xi_1 \quad (54)$$

$$\bar{u}_2^n(0, s) = A_2^n + B_2^n, \quad \bar{\sigma}_2^n(0, s) = A_2^n \eta_2 - B_2^n \eta_2 \quad (55)$$

$$\bar{u}_2^n((1 - \alpha)l, s) = A_2^n \xi_2 + B_2^n / \xi_2, \quad \bar{\sigma}_2^n((1 - \alpha)l, s) = A_2^n \eta_2 \xi_2 - B_2^n \eta_2 / \xi_2 \quad (56)$$

with,

$$\xi_1 = \exp(\gamma_1 \alpha l), \quad \xi_2 = \exp(\gamma_2(1 - \alpha)l) \quad (57)$$

$$\eta_1 = E_1 \gamma_1, \quad \eta_2 = E_2 \gamma_2 \quad (58)$$

The boundary and continuity conditions of displacement and stress fields are used to determine the unknowns A_i^n and B_i^n :

Boundary conditions: $A_1^1 + B_1^1 = 0$ (59)

$$A_2^N \xi_2 + B_2^N / \xi_2 = \hat{u}(s) \quad (60)$$

Displacement continuities: $A_1^n \xi_1 + B_1^n / \xi_1 = A_2^n + B_2^n$ (61)

$$A_2^n \xi_2 + B_2^n / \xi_2 = A_1^{n+1} + B_1^{n+1} \quad (62)$$

Stress continuities: $A_1^n \eta_1 \xi_1 - B_1^n \eta_1 / \xi_1 = A_2^n \eta_2 - B_2^n \eta_2$ (63)

$$A_2^n \eta_2 \xi_2 - B_2^n \eta_2 / \xi_2 = A_1^{n+1} \eta_1 - B_1^{n+1} \eta_1 \quad (64)$$

Equations 59 - 64 are expressed in the following matrix form:

$$\mathbf{MX} = \mathbf{F} \quad (65)$$

verification of the nonlocal homogenization model.

4.3 Inverse Laplace transform

Since all the associated fields are derived in the Laplace domain, it is necessary to transform the response fields into the time domain. The numerical inverse Laplace Transform Method (Brancik, 1999), which is based on Fast Fourier Transform and the ϵ -error algorithm (Macdonald, 1964) is used for transforming the response fields to the time domain. The inverse Laplace Transform is defined as,

$$f(t) = \frac{1}{2\pi i} \int_{c-i\infty}^{c+i\infty} F(s)e^{st} ds \quad (71)$$

with the assumptions that, $|f(t)| \leq Ke^{\beta t}$, where, K is real and positive; $t > 0$; and $\text{Re}(s) > \beta$. The numerical inverse Laplace transform is computed by N_v -term truncation, $\mathbf{F}_{(N_v)}$ of the transformed function values of $F(s)$, with the subscript N_v denoting the dimension of the vector:

$$\mathbf{f}_{(M_v)} = \mathbf{C}_{(M_v)} \circ \{2\text{Re} [\mathcal{E}(\text{FFT}(\mathbf{F}_{(N_v)}))] - \mathbf{F}_{0(M_v)}\} \quad (72)$$

where, \circ denotes the Hadamard product of matrices, e.g. the element-by-element product; $\mathcal{E}(\cdot)$ represents the ϵ -error algorithm, and $\mathbf{F}_{0(M_v)}$ is a M_v -element constant vector of c which can be computed as,

$$c = \beta - \frac{\Omega}{2\pi} \ln E_r \quad (73)$$

$$\Omega = \pi(1 - 1/M_v)/t_m \quad (74)$$

where $t_m = (M_v - 1)T_s$ and $M_v = N_v/2$. T_s is the sampling period in the time domain, E_r the desired relative error, and:

$$\mathbf{C}_{(M_v)}(k) = \frac{\Omega}{2\pi} \exp(ckT_s) \quad (75)$$

$$\mathbf{F}_{(N_v)}(n) = F(c - in\Omega) \quad n = 0, 1, \dots, N_v - 1 \quad (76)$$

A more detailed description of the inverse Laplace transform method is presented by Brancik (1999).

4.4 Dissipated energy

The rate of dissipated energy density for the viscoelastic material model using the Duhamel's integral takes the following form (Fung, 1965):

$$\dot{W}_d(x, y, t) = \int_0^t \int_0^t -\dot{g}(x, y, 2t - \tau_1 - \tau_2) \epsilon_{,\tau_1}(x, y, \tau_1) \epsilon_{,\tau_2}(x, y, \tau_2) d\tau_1 d\tau_2 \quad (77)$$

Equation 77 requires the computation of strain field in the time domain. In the Laplace domain, the associated macroscopic strain, $\bar{\epsilon}$ is related to the associated displacement field as follows,

$$\bar{\epsilon}(x, y, s) = \bar{u}_{,x} \quad (78)$$

Substituting Eq. 19 and the linearizations of \bar{u}_1 , \bar{u}_2 , and, \bar{u}_3 (i.e. Eqs. 25, 37) and 40, into Eq. 78, we can simplify the expression for associated strain:

$$\bar{\epsilon}(x, y, s) = (1 + H_{,y})\bar{U}_{,x} + \zeta(H + P_{,y})\bar{U}_{,xx} + \zeta^2(P + Q_{,y})\bar{U}_{,xxx} + O(\zeta^3) \quad (79)$$

in which, the localization functions, $(1 + H_{,y})$, $(H + P_{,y})$ and $(P + Q_{,y})$ are readily available through differentiation of the influence functions and provided in Appendix A.

The reference solution provides the associated strain of phase i in microstructure Ω_i^n as:

$$\bar{\epsilon}_i^n(x_i, y, s) = A_i^n \gamma_i \exp(\gamma_i x_i) - B_i^n \gamma_i \exp(-\gamma_i x_i) \quad i = 1, 2 \text{ and } n = 1, 2, \dots, N \quad (80)$$

The rate of dissipated energy density is evaluated by inverting the associated strain and substituting it into the real time domain using the numerical inverse Laplace transform.

Table 1: Viscoelastic material parameters for polyurea (Amirkhizi et al., 2006).

k_1 [MPa]	k_2 [MPa]	k_3 [MPa]	k_4 [MPa]	k_e [MPa]
37.8918	75.5328	161.0112	194.5216	44.8
q_1 [ms]	q_2 [ms]	q_3 [ms]	q_4 [ms]	ρ [kg/m ³]
463.4	0.06407	1.163×10^{-4}	7.321×10^{-7}	1070

5 Numerical Examples

A series of simulations have been conducted to assess the validity of the proposed nonlocal homogenization model and investigate the energy dissipation characteristics of bimaterial composites as a function of microstructural configuration. The capabilities of the model is verified against the analytical solution of the original single scale boundary value problem and the classical local homogenization model.

The material moduli function that represents the material properties at the scale of microstructure is modeled as:

$$g(y, t) = \begin{cases} E_1 & \text{if } y \in \Theta^{(1)} \\ k_e + \sum_{i=1}^n k_i e^{-t/q_i} & \text{if } y \in \Theta^{(2)} \end{cases} \quad (81)$$

where n is number of Prony series. In all cases below, the first phase is taken to be elastic, whereas the second phase is viscoelastic, modeled by a Prony series approximation. The viscoelastic material idealizes the response of the polyurea material. The material properties of polyurea is provided by Amirkhizi et al. (2006) and summarized in Table 1. Applying the Laplace transform to the modulus function yields:

$$E(y, s) = \begin{cases} E_1 & \text{if } y \in \Theta^{(1)} \\ E_2(s) = k_e + \sum_{i=1}^n \frac{k_i s}{s + \frac{1}{q_i}} & \text{if } y \in \Theta^{(2)} \end{cases} \quad (82)$$

The dissipated energy computations are conducted by taking advantage of the Prony series

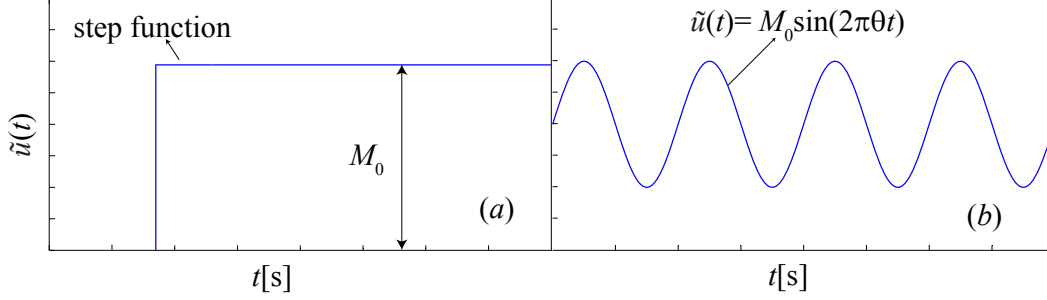


Figure 2: Applied boundary conditions.

approximation. The rate of dissipated energy at the viscoelastic phase is expressed as:

$$\dot{W}_d(x, t) = \sum_{i=1}^n \frac{k_i}{q_i} \epsilon_d^i(x, t) \dot{\epsilon}_d^i(x, t) \quad (83)$$

where,

$$\epsilon_d^i(x, t) = \int_0^t \exp(-(t - \tau)/q_i) \dot{\epsilon} d\tau \quad (84)$$

5.1 Model verification: dispersion and dissipation

In this section, we verify the capability of the nonlocal homogenization model (NHM) in capturing the energy dissipation and dispersion under dynamic loadings. The response of NHM is compared to the classical homogenization model (CHM) and the analytical solution of the reference model (AS). The ratio of the macroscopic and microscopic domain sizes (i.e., N) is set as 40. The modulus of the elastic phase (phase 1) is taken as 1 GPa, and the two phases have equal volume fractions (i.e., $\alpha = 0.5$).

First, we consider the response when the end of the bar is subjected to step loading with magnitude M_0 as illustrated Fig. 2a. We evaluate the response of the bars with four different density contrast in the microstructure (i.e., $\phi = \rho_1/\rho_2 = 1, 2, 5, 10$). The normalized displacement histories as a function of the normalized time (i.e., t/T where, T denotes the observation duration) are shown in Fig. 3 for the four density ratios as computed using NHM, CHM and the reference solutions. The displacement histories are recorded at $0.82L$ distance from the fixed end of the bar. The “cycles” observed in Fig. 3 are due to the repeated reflections of the wave at the fixed and loaded boundaries of the domain. In Figs. 3a-d, the distance between

the displacement peak and trough at each cycle reduces, indicating progressive attenuation of the wave. At the asymptote of complete attenuation, the normalized displacement at the control point approaches 0.82. This corresponds to the uniform strain state induced by a quasi-statically applied unit displacement at the loaded end. At all density ratios, the results indicate good agreement between the nonlocal homogenization approach and the reference solution. Figures 3a-d illustrate that the wave dispersion increases with the density ratio in the microstructure. While the nonlocal model accurately accounts for the wave dispersion at high density ratios, the classical homogenization model fails to capture the wave dispersions. Yet, the dissipation patterns are accurately captured by CHM, which indicates that the attenuation induced by wave dispersion is relatively small. In other words, the dispersion induced attenuation can only be captured by taking account of the higher order derivative term in NHM, however the viscoelastic dissipation resulting from the viscoelastic modulus is included in both the NHM and CHM.

In the simulations displayed in Fig. 3, the density ratios of (i.e., $\phi = 1, 2, 5, 10$) are set by increasing the density of the elastic constituent, ρ_1 , while keeping the density of the viscoelastic constituent, ρ_2 , constant. The density of the homogenized constituent, ρ_0 , in Eq. 34 therefore increases as ϕ is increased, leading to lower wave velocity of the homogenized domain and slower propagation. The effect of dispersion induced internal scattering on the propagation rate at high density ratios is relatively minor. This is because the CHM model is able to capture the slower propagation of the wave at high density ratios accurately, despite missing the dispersion effects.

Next, we investigate the response of the bar when subjected to sinusoidal loading as illustrated in Fig. 2b. The applied loadings is parameterized by the magnitude, M_0 and the frequency, θ . The density ratio, ϕ of the heterogeneous bar is set to 10. Figure 4 shows the normalized displacement history for identical heterogeneous bars vibrating at four different frequencies ($\theta = 10, 30, 50$, and 70 Hz) recorded at $0.82L$ distance from the fixed end of the specimen. At relatively low frequency loading (e.g., $\theta = 10$ Hz), the classical and the nonlocal homogenization models capture the response reasonably accurately, with the exception of the phase shift and accompanying reduction in the peak amplitude originating from the wave re-

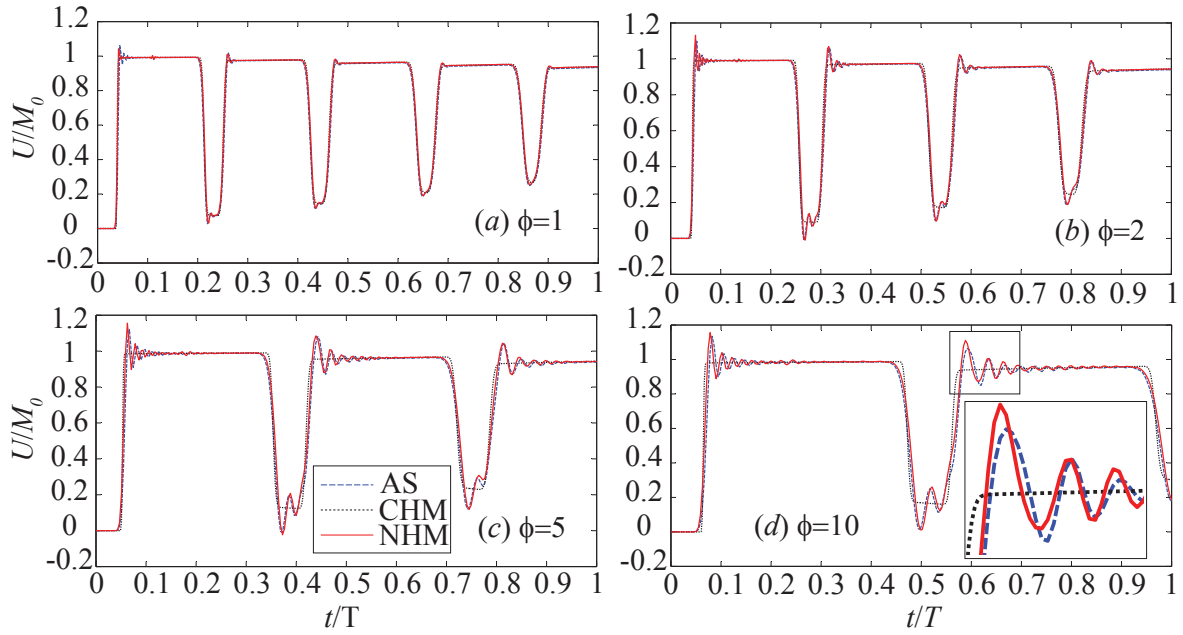


Figure 3: Displacement histories under different density ratios when subjected to step loading.

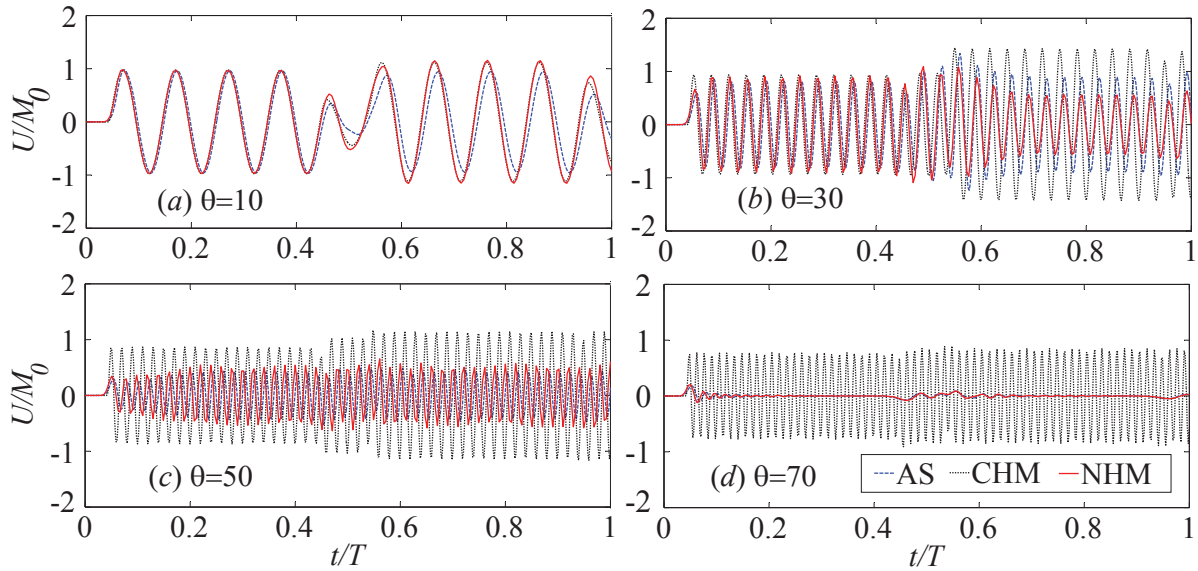


Figure 4: Displacement histories under different loading frequencies when subjected to sinusoidal loading.

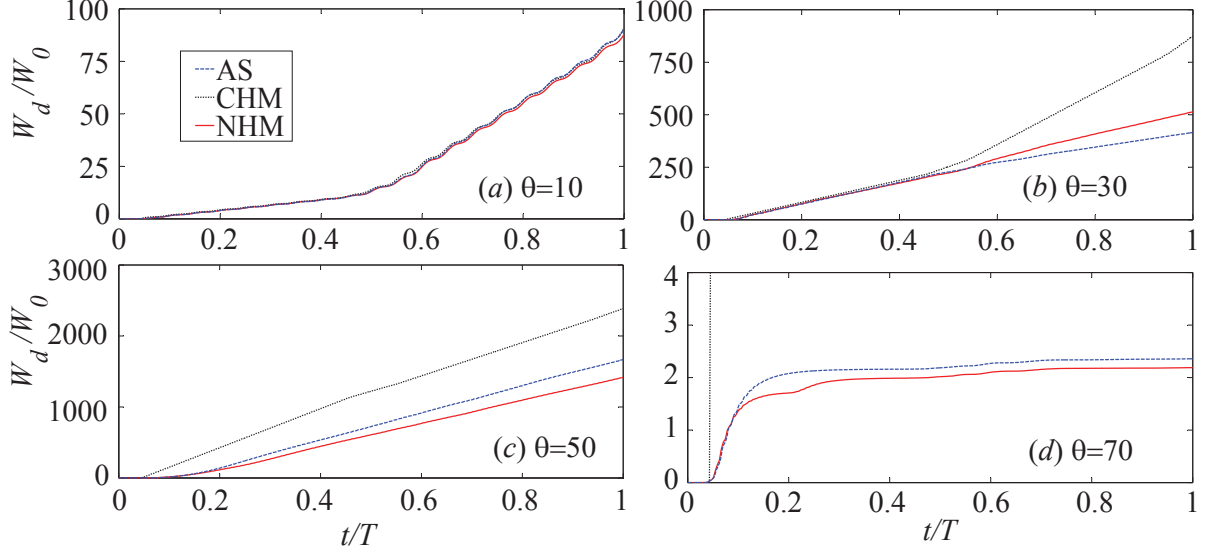


Figure 5: Dissipated energy density histories under different loading frequencies.

flections at the fixed end. At higher frequency loading ($\theta = 30 - 50$ Hz), the attenuation due to heterogeneity induced wave dispersions becomes significantly more pronounced since the shorter wavelength events reflect at the bimaterial interfaces, dissipating energy in the viscous phase. At the highest considered frequency (i.e., $\theta = 70$ Hz), the wave dissipates within a short distance from the applied loading. CHM clearly cannot predict such a attenuation phenomena as apparent in Fig. 4. At high frequency loading, the microscopic dynamics is critical for accurate modeling of dispersive behavior. These observations are reinforced by the dissipated energy density comparison computed at the inspection point on the bar ($0.82L$ distance from the fixed end of the specimen) under sinusoidal loadings as shown in Figure 5. The energy dissipation prediction by NHM is in reasonable agreement with the reference solution for the entire applied loading frequency range, whereas CHM is applicable only for low frequency loadings. The overprediction of dissipation density by CHM at high frequencies at the inspection location reflects the presence of spurious high amplitude waves traveling through the material. The nonlocal model dissipates all high frequency waves prior to reaching the inspection point.

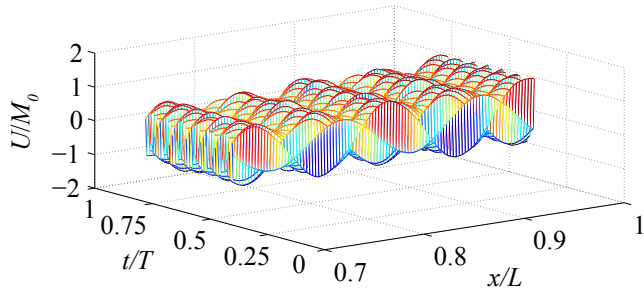
In addition to the favorable accuracy of the nonlocal homogenization model demonstrated above, it is computationally significantly more efficient compared to the reference simulation. While NHM employs a single equilibrium equation in the evaluation of the dynamics response,

the reference model requires the solution of a $4N \times 4N$ system of equations leading to significant computational cost. For instance, when 500 microstructures are included in the problem (i.e., $N = 500$), the computational time required to solve the reference problem is three orders of magnitude larger than the nonlocal model. Such an analysis required approximately two minutes computation time for the nonlocal homogenization model using a single workstation, whereas several days were required to complete the same analysis based on the reference solution. This drawback makes using the analytical solution for simulating responses in structures having a large number of microstructures intractable, and the nonlocal homogenization is favorable compared to the CHM and the reference solution by providing accurate predictions at both scales while maintaining satisfactory time efficiency.

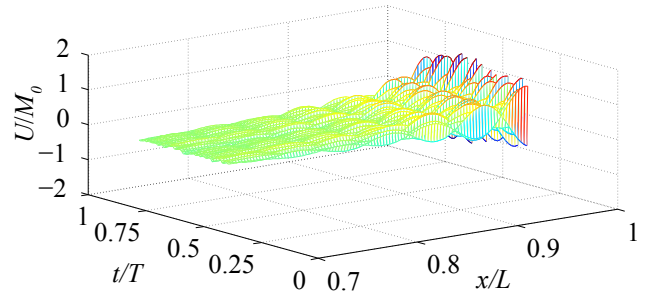
5.2 Effect of microstructure on energy dissipation

In this section, we investigate the dispersive-dissipative wave propagation response for the effect of microstructure on the energy dissipation characteristics. A steel-polyurea composite bar is considered. The material properties of the viscoelastic polyurea phase are summarized in Table 1. The density and modulus of the elastic steel phase are set to $\rho_1 = 7847 \text{ kg/m}^3$ and $E_1 = 200 \text{ GPa}$, respectively. The bar is subjected to a sinusoidal loading with the loading frequency of $\theta = 80 \text{ Hz}$. The ratio of the macroscopic and microscopic domain sizes is set as $N = 20$. The dynamics response of the composite is investigated for six microstructural configurations ($\alpha = 0.1, 0.25, 0.4, 0.6, 0.75$ and 0.9). Nonlocal homogenization model is employed to predict the responses.

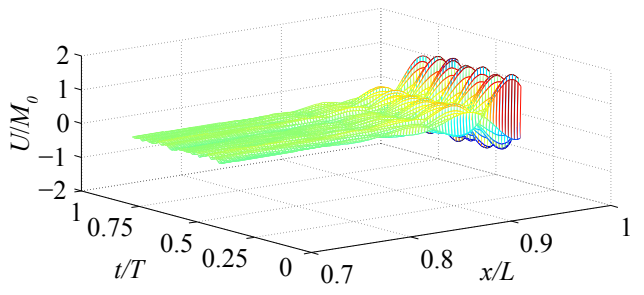
Figure 6 displays the normalized displacement profiles as a function of time and position for the duration of the dynamic loading. When the microstructure consists largely of the polyurea or the steel phase (i.e., $\alpha = 0.1$ and $\alpha = 0.9$, respectively), wave propagation extends throughout the length of the bar. The energy dissipation in the polyurea dominated bar (i.e., $\alpha = 0.1$) is observed at further distance from the excited boundary, whereas small amount of dissipation is observed in the steel dominated bar (i.e., $\alpha = 0.9$). For intermediate configurations with comparable polyurea and steel volume fractions (i.e., $\alpha = 0.25, 0.4, 0.6$ and 0.7), the propagation attenuates within approximately a tenth of the bar, pointing to strong dissipation



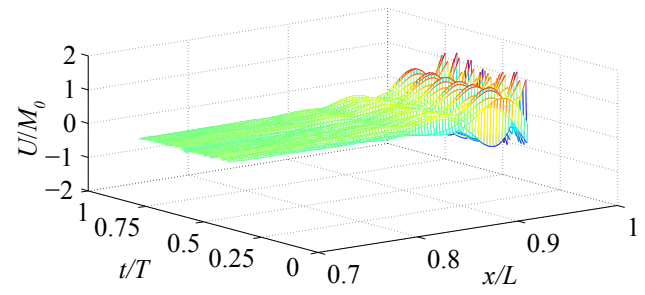
(a) $\alpha = 0.1$



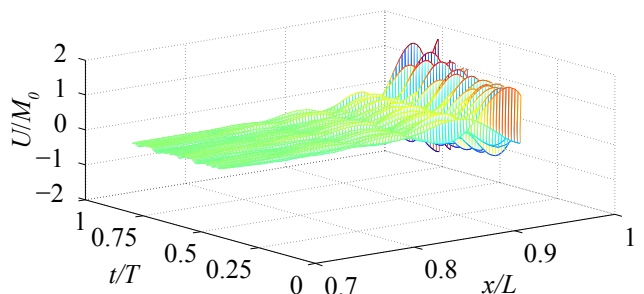
(b) $\alpha = 0.25$



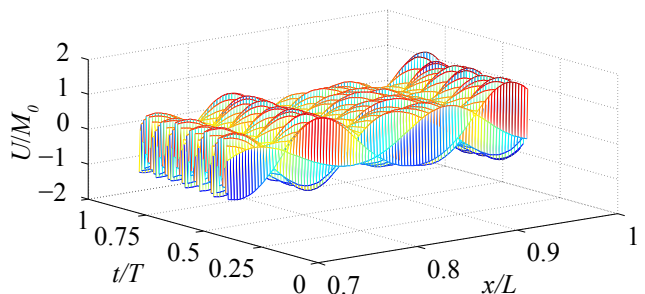
(c) $\alpha = 0.4$



(d) $\alpha = 0.6$



(e) $\alpha = 0.75$



(f) $\alpha = 0.9$

Figure 6: Macrostructural analysis of the displacements for different microstructures.

characteristics activated by the microstructural configuration. The results indicate that the energy dissipation characteristics of the composite steel-polyurea system with balanced volume fractions are even more favorable than configurations dominated by the viscous polyurea phase.

6 Conclusion

This manuscript presented a nonlocal dispersive model for the dynamic response of viscoelastic heterogeneous materials. The proposed model is based on the mathematical homogenization theory with multiple spatial scales applied in the Laplace domain. Asymptotic expansions of the response fields of up to fourth order are included in the homogenization formulation to account for the wave dispersions induced by the microstructural heterogeneity. Numerical verifications indicate that the proposed nonlocal model accurately accounts for the dispersion and dispersion induced attenuation under a wide range of loading and material parameters, which cannot be modeled using the classical homogenization models. In addition, the nonlocal homogenization model provides a high level of computational efficiency by eliminating the temporal and microscopic coordinates. The nonlocal model is used to demonstrate that the microstructural configuration may have a significant impact on the energy dissipation characteristics of heterogeneous materials under dynamic loading conditions.

From the modeling point of view, additional challenges remain that will be addressed in the near future. The model is developed in the context of one-dimensional problems, and will be generalized to the higher dimensions. Extending the proposed approach to higher dimensions requires computational methods rather than the analytical solutions derived in this manuscript, due to the complexity of microstructures. Extending the model to higher dimensions naturally opens the possibility of exploring a wider parameter space of microstructure design for devising microstructural configurations with favorable energy dissipation characteristics.

Acknowledgments

The financial support of the National Science Foundation, CMMI Hazard Mitigation and Structural Engineering program (Grant #:0856168) is gratefully acknowledged.

Bibliography

- I. Abu-Alshaikh, D. Turhan, and Y. Mengi. Propagation of transient out-of-plane shear waves in viscoelastic layered media. *Int. J. Mech. Sci.*, 43:2911–2928, 2001.
- A. V. Amirkhizi, J. Isaacs, J. McGee, and S. Nemat-Nasser. An experimentally-based viscoelastic constitutive model for polyurea, including pressure and temperature effects. *Philos. Mag.*, 86:5847–5866, 2006.
- I. V. Andrianov, V. I. Bolshakov, V. V. Danishevs' kyy, and D. Weichert. Higher order asymptotic homogenization and wave propagation in periodic composite materials. *Proc. R. Soc. Lond. A*, 464:1181–1201, 2008.
- N. S. Bakhvalov and M. E. Eglit. Equations of higher order of accuracy describing the vibrations of thin plates*. *J. Appl. Math. Mech.*, 69(4):593–610, 2005.
- N. S. Bakhvalov and G. Panasenko. Homogenisation: averaging processes in periodic media (mathematical problems in the mechanics of composite materials). *Recherche*, 67:02, 1989.
- T. Bennett, I. M. Gitman, and H. Askes. Elasticity theories with higher-order gradients of inertia and stiffness for the modelling of wave dispersion in laminates. *Int. J. Fract.*, 148:185–193, 2007.
- A. Bensoussan, J. L. Lions, and G. Papanicolaou. *Asymptotic analysis for periodic structures*, volume 5. North Holland, Amsterdam, 1978.
- L. Brancik. Programs for fast numerical inversion of laplace transforms in matlab language environment. *Sbornik 7. Proc. Matlab 99, Prague*, pages 27–39, 1999.

- W. Chen and J. Fish. A dispersive model for wave propagation in periodic heterogeneous media based on homogenization with multiple spatial and temporal scales. *ASME J. Appl. Mech.*, 68:153–161, 2001.
- S. Chin-Teh. Transient rotary shear waves in nonhomogeneous viscoelastic media. *Int. J. Solids Struct.*, 7:25–37, 1971.
- E. Cosserat and F. Cosserat. *Theorie des Corps Deformables*. Hermann & Fils, Paris, France., 1909.
- R. Crouch and C. Oskay. Symmetric mesomechanical model for failure analysis of heterogeneous materials. *Int. J. Multiscale Comput. Eng.*, 8(5):447–461, 2010.
- J. Engelbrecht, A. Berezovski, F. Pastrone, and M. Braun. Waves in microstructured materials and dispersion. *Philos. Mag.*, 85:4127–4141, 2005.
- C. Eringen and E. S. Suhubi. Nonlinear theory of micro-elastic solids II. *Int. J. Eng. Sci.*, 2: 189–203, 1964.
- J. Fish and W. Chen. Higher-order homogenization of initial/boundary-value problem. *J. Eng. Mech.*, 127:1223–1230, 2001.
- J. Fish, W. Chen, and G. Nagai. Non-local dispersive model for wave propagation in heterogeneous media: multi-dimensional case. *Int. J. Numer. Methods Eng.*, 54:347–363, 2002a.
- J. Fish, W. Chen, and G. Nagai. Non-local dispersive model for wave propagation in heterogeneous media: one-dimensional case. *Int. J. Numer. Methods Eng.*, 54:331–346, 2002b.
- Y. Fung. *Foundations of solid mechanics*. Prentice Hall, Englewood Cliffs, New Jersey, 1965.
- S. Gonella, M. S. Greene, and W.K. Liu. Characterization of heterogeneous solids via wave methods in computational microelasticity. *J. Mech. Phys. Solids*, 59:959–974, 2011.
- J. M. Guedes and N. Kikuchi. Preprocessing and postprocessing for materials based on the homogenization method with adaptive finite element methods. *Comput. Meth. Appl. Mech. Eng.*, 83(2):143–198, 1990.

- Y. Jiangong. Viscoelastic shear horizontal wave in graded and layered plates. *Int. J. Solids Struct.*, 48:2361–2372, 2011.
- J. R. Macdonald. Accelerated convergence, divergence, iteration, extrapolation, and curve fitting. *J. Appl. Phys.*, 35:3034–3041, 1964.
- R. D. Mindlin. Micro-structure in linear elasticity. *Arch. Ration. Mech. Anal.*, 16:51–78, 1964.
- S. Mukherjee and E. H. Lee. Dispersion relations and mode shapes for waves in laminated viscoelastic composites by finite difference methods. *Comput. Struct.*, 5:279–285, 1975.
- T. Naciri, P. Navi, and A. Ehrlacher. Harmonic wave propagation in viscoelastic heterogeneous materials part i: Dispersion and damping relations. *Mech. Mater.*, 18:313–333, 1994.
- A. H. Nayfeh. Discrete lattice simulation of transient motions in elastic and viscoelastic composites. *Int. J. Solids Struct.*, 10:231–242, 1974.
- C. Oskay and J. Fish. Eigendeformation-based reduced order homogenization for failure analysis of heterogeneous materials. *Comput. Meth. Appl. Mech. Eng.*, 196:1216–1243, 2007.
- A. V. Porubov, E. L. Aero, and G. A. Maugin. Two approaches to study essentially nonlinear and dispersive properties of the internal structure of materials. *Phys. Rev. E*, 79:046608, 2009.
- M. B. Rubin, P. Rosenau, and O. Gottlieb. Continuum model of dispersion caused by an inherent material characteristic length. *J. Appl. Phys.*, 77:4054–4063, 1995.
- E. Sánchez-Palencia. *Non-homogeneous media and vibration theory*, volume 127. Springer-Verlag, Berlin, 1980.
- F. Santosa and W. W. Symes. A dispersive effective medium for wave propagation in periodic composites. *SIAM J. Appl. Math.*, 51:984–1005, 1991.
- K. Terada and N. Kikuchi. Nonlinear homogenization method for practical applications. In S. Ghosh and M. Ostoja-Starzewski, editors, *Computational Methods in Micromechanics*, volume AMD-212/MD-62, pages 1–16. ASME, 1995.

T. C. T. Ting. The effects of dispersion and dissipation on wave propagation in viscoelastic layered composites. *Int. J. Solids Struct.*, 16:903–911, 1980.

L. Tsai and V. Prakash. Structure of weak shock waves in 2-d layered material systems. *Int. J. Solids Struct.*, 42:727–750, 2005.

Z.-P. Wang and C. T. Sun. Modeling micro-inertia in heterogeneous materials under dynamic loading. *Wave Motion*, 36:473–485, 2002.

A Higher order terms

The localization functions: $1 + H_{1,y}(y, s)$, $H(y, s) + P_{1,y}(y, s)$ and $P(y, s) + Q_{1,y}(y, s)$ in Eq. 79 are derived and shown as follows:

$$1 + H_{1,y}(y, s) = \frac{E_0}{E_1} \quad (\text{A.1})$$

$$1 + H_{2,y}(y, s) = \frac{E_0}{E_2} \quad (\text{A.2})$$

$$H_1(y, s) + P_{1,y}(y, s) = \frac{E_0(1 - \alpha)(\rho_1 - \rho_2)}{2\rho_0 E_1} (2y - \alpha \hat{l}) \quad (\text{A.3})$$

$$H_2(y, s) + P_{2,y}(y, s) = \frac{E_0 \alpha (\rho_1 - \rho_2)}{2\rho_0 E_2} ((1 + \alpha) \hat{l} - 2y) \quad (\text{A.4})$$

$$P_1(y, s) + Q_{1,y}(y, s) = \frac{E_0^2(1 - \alpha) [E_1(-2\rho_1 + \rho_0) + E_2(\rho_1 + \rho_2 - \rho_0)]}{2\rho_0 E_1^2 E_2} (y^2 - \alpha \hat{l} y) - \frac{E_0^3(1 - \alpha) \alpha \hat{l}^2}{12\rho_0 E_1^3 E_2^2} \cdot$$

$$[(1 - \alpha)^2 E_1^2 + \alpha^2 E_2^2] (\rho_0 - \rho_1 - \rho_2) - E_1 E_2 ((2\alpha^3 - 4\alpha^2 + \alpha) \rho_1 - (2\alpha^3 - 2\alpha^2 - \alpha + 1) \rho_2)] \quad (\text{A.5})$$

$$P_2(y, s) + Q_{2,y}(y, s) = \frac{E_0^2 \alpha [E_1(\rho_0 - \rho_1 - \rho_2) + E_2(2\rho_2 - \rho_0)]}{2\rho_0 E_1 E_2^2} ((\hat{l} + \alpha \hat{l}) y - y^2) + \frac{E_0^3 \alpha \hat{l}^2}{12\rho_0 E_1^2 E_2^3} \cdot$$

$$[(-1 - 3\alpha + 3\alpha^2 + \alpha^3) (\rho_0 - \rho_1 - \rho_2) E_1^2 + \alpha^2 ((1 + 4\alpha + \alpha^2) \rho_1 - (6 + 5\alpha + \alpha^2) \rho_2) E_2^2$$

$$+ E_1 E_2 ((\alpha + 7\alpha^2 - 6\alpha^3 - 2\alpha^4) \rho_1 + (-1 - 4\alpha + \alpha^2 + 8\alpha^3 + 2\alpha^4) \rho_2)] \quad (\text{A.6})$$